Supporting information for

Enhanced electrolytic oxygen evolution by the synergistic effects of trimetallic FeCoNi boride oxides immobilized on polypyrrole/reduced graphene oxide

Hui Mao[a], Xi Guo[a], Yuanlin Fu[a], Haoran Yang[a], Yu Zhang[a], Rui Zhang[a, b] * and Xi-Ming Song[a] *

[a] Liaoning Key Laboratory for Green Synthesis and Preparative Chemistry of Advanced Materials, College of Chemistry, Liaoning University, Shenyang 110036, China

[b] College of Pharmaceutical Engineering, Shen Yang Pharmaceutical University, Shenyang 110016, P.R. China

*Author to whom any correspondence should be addressed.

Tel.: 86-24-62202378; Fax: 86-24-62202380

E-mail: *ruizhang@lnu.edu.cn* (R. Z.) and *songlab@lnu.edu.cn* (X. M. S.)

Numbers of pages: 8

Experimental Section

Materials: Pyrrole (Py) (≥98.0%), $NaBH_4$ (≥96.0%) and high-purity graphite powder (≥99.85%) are chemical grade, which were purchased from Sinopharm Chemical Reagent Co. Ltd.. All the other reagents were analytical grade and used without further purification, such as $KMnO_4$ (Tianjin Baishi Chemical Co. Ltd, ≥99.5%), $FeCl_3 \cdot 6H_2O$ (≥99.0%), $CoCl_2.6H_2O$ (≥99.0%), $NiCl_2.6H_2O$ (≥99.0%) and H_2SO_4 (≥98.3%) (Sinopharm Chemical Reagent Co. Ltd.), ethanol (≥99.7%) (Tianjin Yongda Chemical Reagent Co., Ltd.), IrO_2 (Aladdin reagent (Shanghai) Co., Ltd., ≥99.9%), H_2O_2 (Shenyang Xinhua Reagent Factory, ≥30.0%), KOH (Tianjin Damao Chemical Factory, ≥85.0%) and $NaNO_3$ (Tianjin Bodi Chemicals Co., Ltd., ≥99.0%).

Characterizations and Apparatus: The morphology and size of $FeCoNiBO_x$/PPy/rGO nanocomposites were determined with scanning electron microscopy (SEM) measurements (performed on a Hitachi SU-8010 electron microscope with primary electron energy of 10 kV) and transmission electron microscopy (TEM) measurements (performed on a JEM-2100 electron microscope (JEOL, Japan) equipped with a CCD camera at an acceleration voltage of 200 kV). The chemical composition of $FeCoNiBO_x$/PPy/rGO was determined by energy dispersive spectroscopy (EDS) measurement via EDAX-TEAM™ EDS (USA) integrated on the SEM (Hitachi, SU-8010). X-Ray Diffraction (XRD) patterns were obtained with a D8 AXS diffractometer (Bruker, GER) using Cu Kα radiation. Fourier transform infrared (FTIR) spectra of KBr powder-pressed pellets were recorded on a PerkinElmer Spectrum One FTIR spectrometer (PerkinElmer Corp., USA). Raman measurements were acquired using an inVia Raman microscope (Renishaw, Gloucestershire, United Kingdom) with excitation laser wavelength at 633 nm. Analysis of the X-ray photoelectron spectra (XPS) was performed on a Kratos Axis Ultra DLD electron spectrometer using a monochromatic Al Kα source operated at 150 W. The weight content of Fe, Co and Ni element in $FeCoNiBO_x$/PPy/rGO nanocomposites were determined by an inductively coupled plasma-optical emission spectrometry (ICP-OES, Agilent 5110, Agilent, USA) after concentrated acids (HNO_3:H_2O_2=7:1, v/v) digestion. The electrochemical performance of $FeCoNiBO_x$/PPy/rGO was investigated by using linear sweep voltammetry (LSV) and cyclic voltammetry (CV) with a CHI660E Electrochemical Station (Shanghai CHENHUA instrument Co., Ltd.). In a three-electrode system, a modified GCE, a platinum wire and an Hg/HgO electrode were used

as the working electrode, the counter electrode and the reference electrode, respectively. The measurements were performed in 1.0 M KOH with IR-compensation. The measured potentials versus Hg/HgO were converted to reversible hydrogen electrode (RHE). The interfacial charge-transfer resistance of samples was determined by using electrochemical impedance spectroscopy (EIS) in the frequency range between 0.01 Hz and 10000 Hz with a perturbation signal of 5 mV.

The measured potentials versus Hg/HgO were converted to RHE scale according to the Nernst equation:

$$E_{RHE} = E_{Hg/HgO} + 0.059pH + 0.098 \quad \text{(Eqs. S1)}$$

The Tafel slope was obtained by LSV curves and calculated according to the following equation:

$$\eta = a + b \log J \quad \text{(Eqs. S2)}$$

where η is the overpotential, J is the current density, and b is the Tafel slope. The overpotential was calculated as follows:

$$\eta = E_{RHE} - 1.23 \quad \text{(Eqs. S3)}$$

Double layer capacitance (C_{dl}) measurements: To measure the electrochemical capacitance, the potential was swept between 1.12 to 1.28 V vs. RHE at different scanning rates (2, 4, 6, 8, 10, 12, 14, 16, 18 and 20 mV s^{-1}) with an assumption of double layer charging in the potential range. The capacitive currents at 1.19 V vs. RHE were measured and plotted as a function of scanning rate. The linear slope of $|\Delta j| = |j_a - j_c|$ against scanning rates was twice the C_{dl}.

Determination of electrochemically active surface area (ECSA): Assume that the specific capacitance (C_s) for a flat surface was about 40 μF cm^{-2} for 1 cm^2 of real surface area,[S1] the ECSA was calculated as follows:

$$ECSA = C_{dl}/C_s \quad \text{(Eqs. S4)}$$

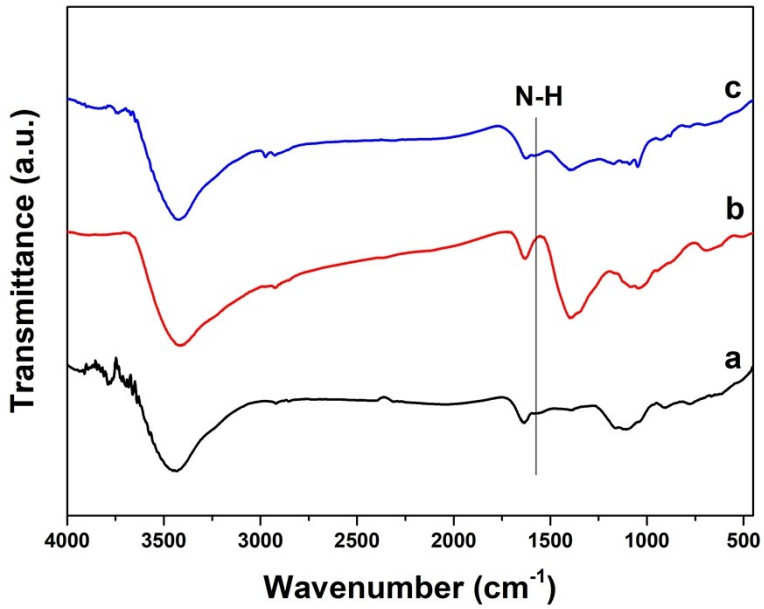

Fig. S1. FTIR spectra of (a) PPy/rGO; (b) $FeCoNiBO_x$ and (c) $FeCoNiBO_x$/PPy/rGO.

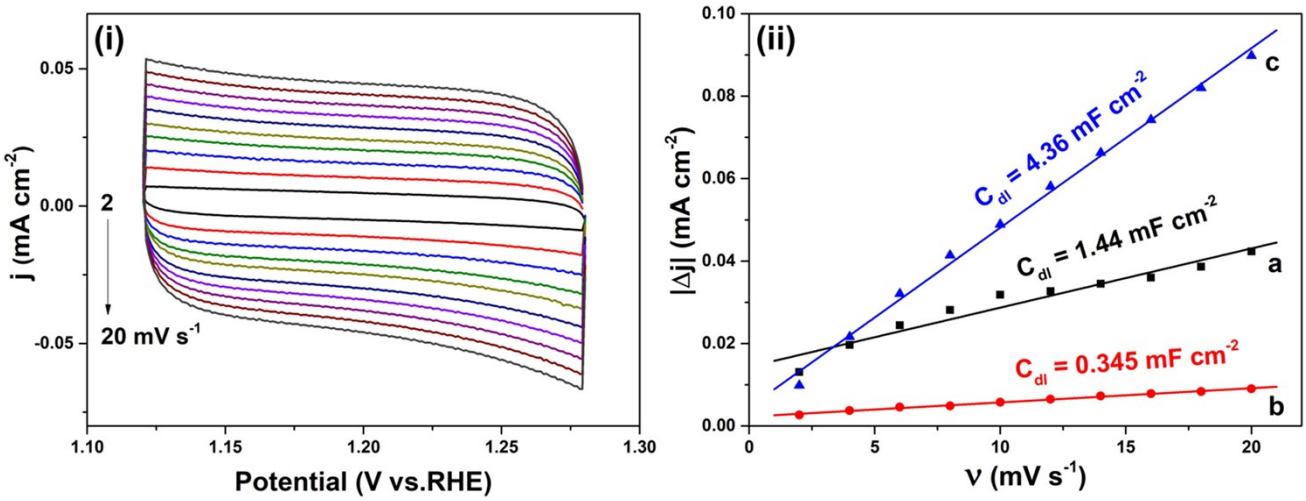

Fig. S2. (i) cyclic voltammograms of $FeCoNiBO_x$/PPy/rGO modified GCE at different scanning rate in the range of 2-20 mV s^{-1} in 1 M KOH with saturated O_2; (ii): plots of anodic peak current density vs. scanning rates from (i) at 1.19 V by (a) $FeCoNiBO_x$, (b) $FeCoNiBO_x$/rGO and (c) $FeCoNiBO_x$/PPy/rGO

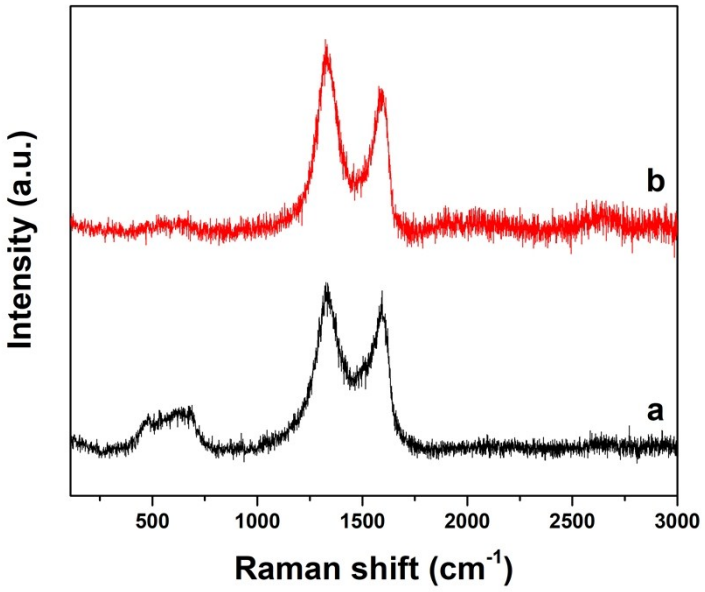

Fig. S3. Raman spectra of $FeCoNiBO_x$/PPy/rGO (a) before and (b) after electrocatalysis for 20 h by chronoamperometry.

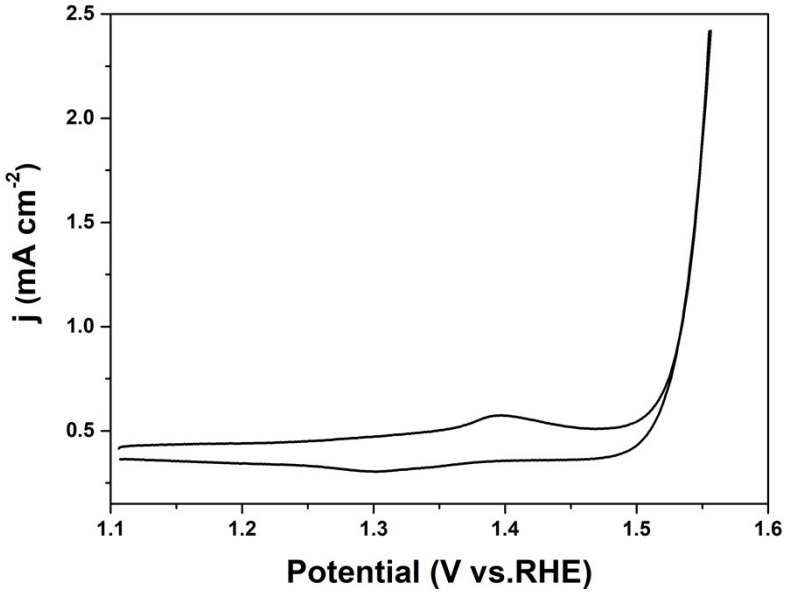

Fig. S4. cyclic voltammograms of $FeCoNiBO_x$/PPy/rGO modified GCE at scanning rate of 10 mV s^{-1} in 1 M KOH with saturated O_2.

Table S1. Comparison of the electrocatalytic OER activity of representative nonprecious OER catalysts in 1.0 M KOH electrolyte.

Electrocatalysts	η_{10} (mV)@ j_a=10 mA cm^{-2}	Tafel slop (mV dec^{-1})	Substrate	Ref.
FeCoNiBO$_x$/PPy/rGO	**290**	**47.0**	**GCE**	**This work**
[a] FeCoNi oxynitride	291	63.8	GCE	S2
[b] FeCoNi-LTH/$NiCo_2O_4$	300	71.5	carbon cloth	S3
[c] FeCo/FeCoNi@NCNTs-HFs	378	57.0	GCE	S4
[d] FeCoNi	300	45.0	nickel foam	S5
[e] FeCoNi@FeNC	330	57.0	GC RDE	S6
[f] FeCoMo	270	63.0	carbon paper	S7
[g] FeCoNi alloys encapsulated in graphene layers	288	60.0	GC RDE	S8
[h] CoFe@NC/rGO	278	52.0	GCE	S9

[a] FeCoNi oxynitride core-shell nanostructures with a homogeneously nitride core and oxide shell

[b] $NiCo_2O_4$ nanoneedles decorated with FeCoNi layered ternary hydroxides

[c] FeCo/FeCoNi/N-doped carbon nanotubes grafted polyhedron-derived hybrid fibers

[d] electrodeposited ternary iron-cobalt-nickel catalyst on nickel foam

[e] ultrathin Fe-N-C nanosheets coordinated Fe-doped CoNi alloy nanoparticles

[f] FeCoMo supported on carbon paper pre-heated at 1000 °C for 1 min

[g] graphene layers encapsulated FeCoNi ternary alloys

[h] metal organic framework derived CoFe@N-doped carbon/reduced graphene sheets

Table S2. The η_{onset}, η_{10} and Tafel slop performance of the products synthesized in this work.

The products	η_{onset} (mV)@ j_a=1 mA cm^{-2}	η_{10} (mV)@ j_a=10 mA cm^{-2}	Tafel slop (mV dec^{-1})
rGO	407	--	183.6
PPy/rGO	400	--	115.1
$FeCoNiBO_x$	297	366	103.6
$FeCoNiBO_x$/rGO	240	311	78.0
$FeCoNiBO_x$/PPy/rGO	**230**	**290**	**47.0**
IrO_2	242	288	48.4
$NiBO_x$/PPy/rGO	350	--	132.5
$FeBO_x$/PPy/rGO	320	390	63.1
$CoBO_x$/PPy/rGO	206	348	112.1
$NiFeBO_x$/PPy/rGO	290	380	85.4
$CoNiBO_x$/PPy/rGO	357	480	78.2
$CoFeBO_x$/PPy/rGO	289	340	63.2

References

S1 X. Li, L. Zhang, M. Huang, S. Wang, X. Li and H. Zhu, *Journal of Materials Chemistry A*, 2016, **4**, 14789.
S2 J. Di, H. Zhu, J. Xia, J. Bao, P. Zhang, S.-Z. Yang, H. Li and S. Dai, *Nanoscale*, 2019, **11**, 7239.
S3 Y. Liu, Y. Bai, Y. Han, Z. Yu, S. Zhang, G. Wang, J. Wei, Q. Wu and K. Sun, *ACS applied materials & interfaces*, 2017, **9**, 36917.
S4 Z. Wang, J. Ang, B. Zhang, Y. Zhang, X. Y. D. Ma, T. Yan, J. Liu, B. Che, Y. Huang and X. Lu, *Applied Catalysis B: Environmental*, 2019, **254**, 26.
S5 Y. Li, S. Yang, H. Li, G. Li, M. Li, L. Shen, Z. Yang and A. Zhou, *Colloids and Surfaces A: Physicochemical and Engineering Aspects*, 2016, **506**, 694.
S6 Q. Zhang, R. F. Webster, S. Cheong, R. D. Tilley, X. Lu and R. Amal, *Particle & Particle Systems Characterization*, 2019, **36**, 1800252.
S7 H. Zhang, J. Zheng, Y. Chao, K. Zhang and Z. Zhu, *New Journal of Chemistry*, 2018, **42**, 7254.
S8 Y. Yang, Z. Lin, S. Gao, J. Su, Z. Lun, G. Xia, J. Chen, R. Zhang and Q. Chen, *ACS Catalysis*, 2016, **7**, 469.
S9 F. Kong, K. Chen, S. Song and D. Xue, *Inorganic Chemistry Frontiers*, 2018, **5**, 1962.